Zhu, H., Shprits, Y., Chen, L., Liu, X., Kellerman, A. C. (2018): An Event on Simultaneous Amplification of Exohiss and Chorus Waves Associated With Electron Density Enhancements. - *Journal of Geophysical Research*, *123*, 11, pp. 8958—8968.

DOI: http://doi.org/10.1029/2017JA025023

Journal of Geophysical Research: Space Physics

RESEARCH ARTICLE
10.1029/2017JA025023

An Event on Simultaneous Amplification of Exohiss and Chorus Waves Associated With Electron Density Enhancements

Hui Zhu[1,2], **Yuri Y. Shprits**[2,3,4], **Lunjin Chen**[1], **Xu Liu**[1], **and Adam C. Kellerman**[2]

[1]Department of Physics, University of Texas at Dallas, Richardson, TX, USA, [2]Department of Earth, Planetary, and Space Sciences, University of California, Los Angeles, CA, USA, [3]Helmholtz Centre Potsdam, GFZ German Research Centre For Geosciences, Potsdam, Germany, [4]University of Potsdam, Potsdam, Germany

Abstract Whistler mode exohiss are the structureless hiss waves observed outside the plasmapause with featured equatorward Poynting flux. An event of the amplification of exohiss as well as chorus waves was recorded by Van Allen Probes during the recovery phase of a weak geomagnetic storm. Amplitudes of both types of the waves showed a significant increase at the regions of electron density enhancements. It is found that the electrons resonant with exohiss and chorus showed moderate pitch angle anisotropies. The ratio of the number of electrons resonating with exohiss to total electron number presented in-phase correlation with density variations, which suggests that exohiss can be amplified due to electron density enhancement in terms of cyclotron instability. The calculation of linear growth rates further supports above conclusion. We suggest that exohiss waves have potential to become more significant due to the background plasma fluctuation.

Key Points:
- Simultaneous amplification of chorus and exohiss is observed by Van Allen Probes
- The plasma analysis of RBSPICE and HOPE suggests that the enhancement of electron number density accounts for the wave amplification
- The calculation of growth rate based on linear theory verifies the importance of density

Correspondence to:
H. Zhu,
zhuhui328@gmail.com

Citation:
Zhu, H., Shprits, Y. Y., Chen, L., Liu, X., & Kellerman, A. C. (2018). An event on simultaneous amplification of exohiss and chorus waves associated with electron density enhancements. *Journal of Geophysical Research: Space Physics*, *123*, 8958–8968. https://doi.org/10.1029/2017JA025023

Received 22 NOV 2017
Accepted 10 OCT 2018
Accepted article online 17 OCT 2018
Published online 5 NOV 2018

1. Introduction

Whistler mode chorus emission is one important type of electromagnetic waves in the terrestrial inner magnetosphere, which usually occurs in the low-electron-density region outside the plasmasphere from magnetic local time (MLT) 22 to 16 (Burtis & Helliwell, 1969; Li, Bortnik, Thorne, & Angelopoulos, 2011; Meredith et al., 2001; Tsurutani & Smith, 1974, 1977). The frequency of chorus waves lies between $0.1f_{ce}$ and $0.8\ f_{ce}$, where f_{ce} is equatorial electron gyrofrequency (Helliwell, 1967; Tsurutani & Smith, 1977). Chorus waves are generally believed to be excited by cyclotron resonant interaction with pitch angle anisotropic electrons with energies ranging from a few to tens of kiloelectron volts (Kennel & Petschek, 1966; Meredith et al., 2001; Nunn et al., 1997). It is widely accepted that chorus emission plays a key role in the rapid acceleration and precipitation loss of radiation belt electrons (Horne & Thorne, 1998; Reeves et al., 2013; Shprits et al., 2008; Summers et al., 2002, 2007; Thorne, 2010; Turner, Angelopoulos, Li, et al., 2014; Turner, Angelopoulos, Morley, et al., 2014; Xiao et al., 2014). Several studies indicate that chorus waves occurring in nightside plasma sheet region are able to scatter kiloelectron volt electrons by means of cyclotron resonance, which is considered to be responsible for the formation of diffuse aurora (Ni et al., 2008; Nishimura et al., 2010).

Structureless hiss waves can be observed outside the plasmasphere, which is referred to as exohiss (Bortnik et al., 2008; Thorne et al., 1973; Zhu et al., 2015). Using Ogo 5 satellite measurement, Thorne et al. (1973) investigated extremely low frequency hiss waves in the magnetosphere and for the first time found that a part of hiss waves appeared outside the plasmasphere in the dayside high-latitude region. They proposed that the source of exohiss is plamaspheric hiss, which is able to leak from the high-density plasmasphere into low-density trough region. The primary occurrence of exohiss in the dayside high-latitude region can be well explained in terms of weak density gradient of the plasmapause. Recently, Zhu et al. (2015) analyzed an exohiss wave event occurring in low latitude recorded by the Electric and Magnetic Field Instrument Suite and Integrated Science (EMFISIS; Kletzing et al., 2013) wave instrument onboard the Van Allen Probes (Mauk et al., 2013). Wave Poynting fluxes pointing toward the equator rather than higher latitude is considered to be a key feature of identification. The MLT-dependent cold electron and suprethermal electron densities corresponding to MLT-dependent exohiss feature further supports the formation mechanism. The corresponding quasi-linear diffusion coefficients suggest the potential pitch angle scattering of relativistic electrons produced by exohiss. However, more comprehensive observation features of exohiss waves are required to verify the formation mechanism and estimate the potential effect on magnetospheric particles.

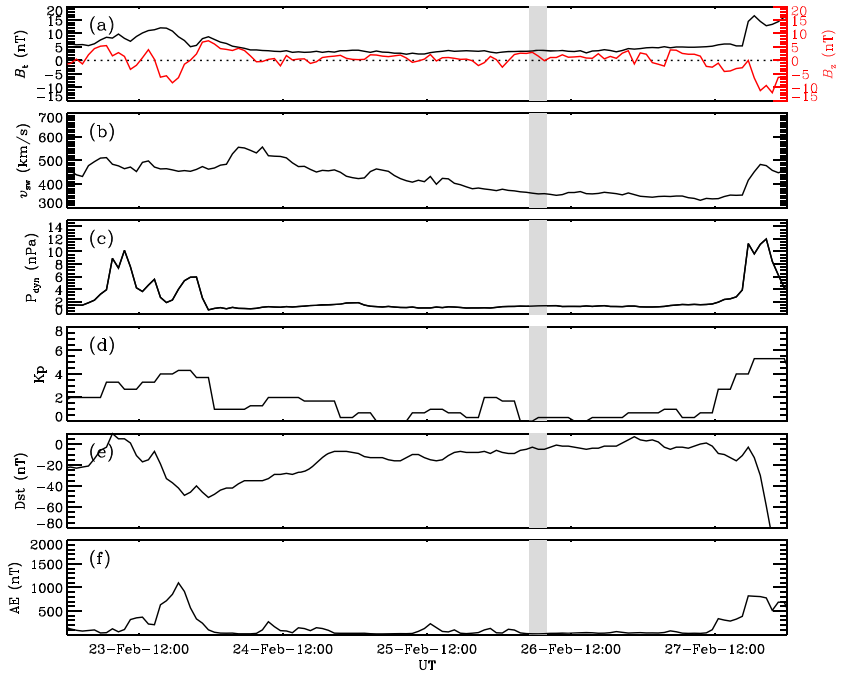

Figure 1. The 23 February 2014 storm event. The gray region indicates the wave event that occurred during the end of the storm. (a) Magnetic intensity (black solid line) and B_Z component (red solid line) in geocentric solar magnetospheric coordinate; (b) solar wind velocity; (c) dynamical pressure of solar wind; (d) Kp index; (e) Dst index; and (f) AE index.

Variation of background electron number density is believed to provide a preferential condition for the amplification of whistler mode emissions. Based on CLUSTER spacecraft data Moullard et al. (2002) reported an electron density fluctuation near the plasmapause, which in-phase modulated the 100–600 Hz emission band but out-of-phase modulated 3–6 kHz band. Chen, Thorne, et al. (2012) studied a modulation of plasmaspheric hiss intensity by plasma density structure, and the calculation of local growth rate suggests that the growth rate increases as the plasma density increases. Its combination with the ray focusing during the wave propagation is responsible for the observed modulation. Li, Bortnik, Thorne, Nishimura, et al. (2011) systematically investigated the role of density variation in the modulation of whistler mode chorus waves and found that both density depletions and density enhancements are correlated with the increase of chorus wave amplitudes. Until now, the modulation of whistler mode exohiss similar to chorus and hiss has not been reported yet.

In this paper, we will report a simultaneous amplification of exohiss and chorus waves correlated with electron density enhancement. The linear theory (Kennel & Petschek, 1966; Xiao et al., 1998) in relativistic plasma is adopted to investigate the possible mechanisms of waves amplification.

2. Observations and Analysis

Figure 1 shows the interplanetary and geomagnetic indices during 23–28 February 2014 obtained from CDAweb-OMNI database. A weak geomagnetic storm occurred starting from 23 February 2014, driven by sudden appearance of strong dynamic pressure and southern interplanetary magnetic field. The minimum of Dst values can reach around −50 nT, and AE index increased up to 1,000 nT during the main phase. We primarily focus on the interval 05:00–08:00 UT on 26 February 2014 when we observed the simultaneous intensification of whistler mode exohiss and chorus waves. This interval is during the late recovery phase of the weak geomagnetic storm, and the Kp and AE indices were very smaller, indicating that geomagnetic and substorm activity is weak.

Figure 2 presents the overview of the event captured by the waves instrument of the EMFISIS suite (Kletzing et al., 2013) onboard the Van Allen Probe A. The upper hybrid resonance frequency (f_{hfr}) line could be visually identified in the electric power spectral density of high-frequency receiver (HFR) channel. The low values of f_{hfr} indicate that during this interval, Probe A was crossing through the plasmatrough. The fluctuation of f_{hfr}

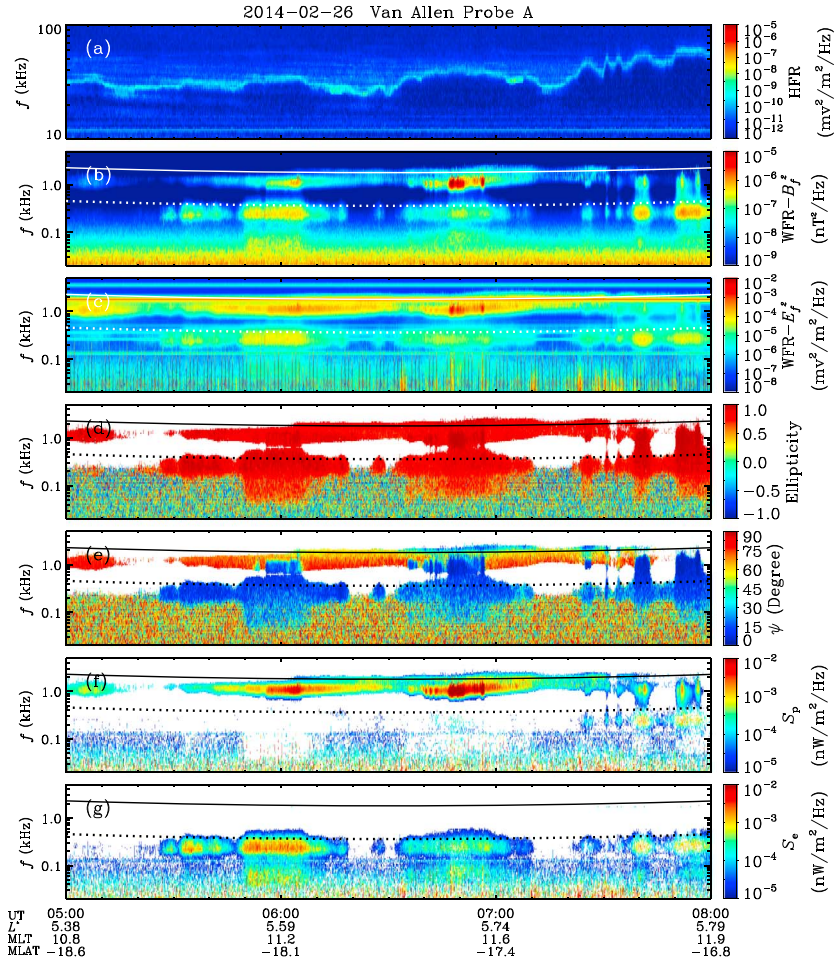

Figure 2. Frequency-time spectrograms of (a) electric power spectral density in the high-frequency receiver (HFR) channel; (b) magnetic and (c) electric power spectral densities in the waveform receiver (WFR) channel; (d) ellipticity of magnetic field polarization; (e) normal angle ψ; (f) poleward Poynting flux; and (g) equatorward Poynting flux. The solid and dotted lines (in all panels except a) indicate $0.5f_{ce}$ and $0.1f_{ce}$. MLT = magnetic local time; MLAT = magnetic latitude.

suggests the in-phase fluctuations of either ambient magnetic intensity or cold electron number density. Two bands of electromagnetic waves were observed in the magnetic and electric power spectral density of waveform receiver (WFR) channel. One band was in the frequency range from $0.1f_{ce}$ to $0.5f_{ce}$, but another band was in the frequency range below $0.1f_{ce}$. Both of the two band waves were predominantly circularly polarized with ellipticity closing to 1 shown in Figure 2d, suggesting that both of the waves can be identified as whistler mode waves. Their wave normal angles presented different characteristics. The normal angels of band below $0.1f_{ce}$ mainly close to zero, indicating the field-aligned propagation feature. While for the band ranging [$0.1f_{ce}$, $0.5f_{ce}$] the normal angle could present either field aligned or obliqueness. The most interesting thing is that the Poynting fluxes of both bands show opposite directions. The Poynting fluxes of band below $0.1f_{ce}$ were pointing equatorward while the Poynting flux of band between [$0.1f_{ce}$, $0.5f_{ce}$] were pointing poleward. Obviously, the band between [$0.1f_{ce}$, $0.5f_{ce}$] is namely whistler mode chorus waves, which are frequently observed outside the plasmasphere in the night sector. Chorus waves are usually generated near the minimum of geomagnetic field (magnetic equator) due to the substorm injection and then propagate toward high latitude. Hence, their Poynting fluxes are poleward. The band below $0.1f_{ce}$ with equatorward Poynting fluxes could be considered as exohiss wave, recently reported by Zhu et al. (2015). The formation of exohiss is believed to result from the leakage of plasmaspheric hiss after excluding the possibilities of excitation at high latitude and bounce propagation of chorus wave (Bortnik et al., 2008; Chen et al., 2012a, 2012b). The schematic figure about the formation of exohiss can be found in Figure 2 of Zhu et al. (2015). Its intensity is partially controlled by the plasmatrough suprathermal electrons via the Landau damping. In this event, we can see both the intensities of exohiss and chorus wave are modulated with the upper hybrid resonance frequency. When

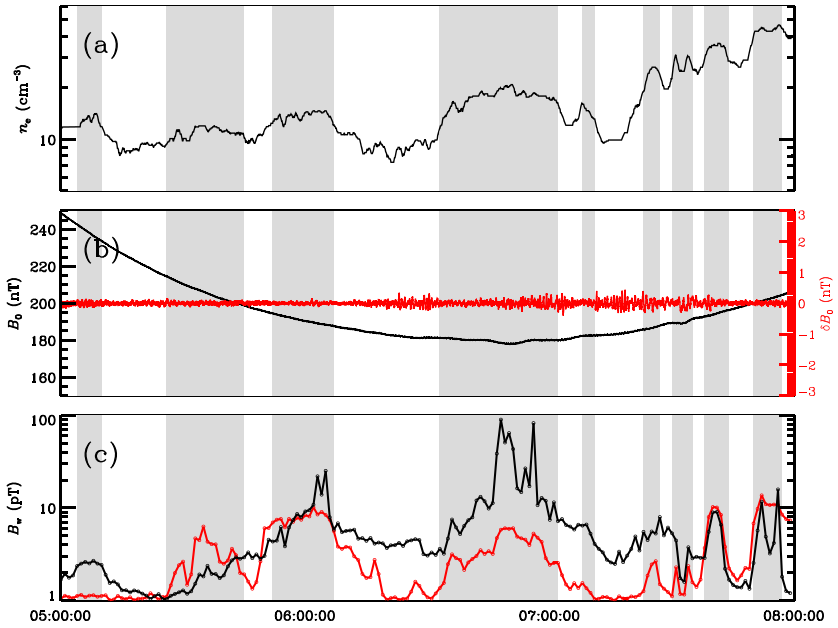

Figure 3. (a) Electron number density derived from high-frequency receiver channel; (b) observed magnetic intensity (black solid line) and fluctuation (red solid line) based on magnetometer instrument; and (c) wave amplitudes. The red and black lines in panel (c) represent the amplitudes in the frequency range [100, 700] and [700, 3000] Hz. The gray regions are selected to highlight the enhancement of electron number density.

upper hybrid resonance frequency line fluctuates toward high frequency, the intensities of exohiss and chorus tend to increase. Particularly, the wave normal angle of chorus shown in Figure 2e also exhibits fluctuations. The wave normal becomes smaller with density enhanced. The upper hybrid resonance frequency is determined by both of electron number density and ambient magnetic intensity. Below we investigate which one is dominated.

Figure 3 shows the obtained electron number density, ambient magnetic field, and wave amplitudes. Here the electron number density is automatically identified based on Neural-network-based Upper hybrid Resonance Determination (NURD) algorithm (Zhelavskaya et al., 2016). The ambient magnetic field was recorded by the fluxgate magnetometer instruments of the EMFISIS. The fluctuation of magnetic field is obtained by subtracting the 100-s-running average magnetic intensity. The wave amplitudes are obtained by integrating the magnetic power spectral density within the corresponding frequency ranges. The frequency range [100, 700] Hz basically represents exohiss, and the range [700, 3000] Hz represents the lower band chorus. We can see that the number density shows the discrete enhancements, which are marked by the gray color. The ambient magnetic field showed a much smaller fluctuation compared with the number density. The wave amplitudes of both exohiss and chorus presented positive correlation with electron number density neither the ambient magnetic intensity nor magnetic fluctuations. When the number density increased, the wave amplitudes simultaneously increased and vice versa. It should be noted that the intensities of higher-frequency range are roughly larger than those of lower-frequency range. The intensities of wave within higher-frequency range can reach 100 pT, and maximum intensity of wave within lower frequency is around 10 pT, which is consistent with previous observation by Zhu et al. (2015). Below we investigate if the density enhancement produces wave amplification and how the density variation works.

We will look into the amplification of exohiss and chorus in the frame of linear theory (Kennel & Petschek, 1966; Xiao et al., 1998). The local growth rate (ω_i) for field-aligned whistler mode wave in a relativistic plasma is

$$\omega_i = \frac{\pi\omega_{pe}^2\eta}{[2\omega_r + \omega_{pe}^2|\Omega_e|/(\omega_r - |\Omega_e|)^2]}\left[A(p_R) - A_c\right], \quad (1)$$

where

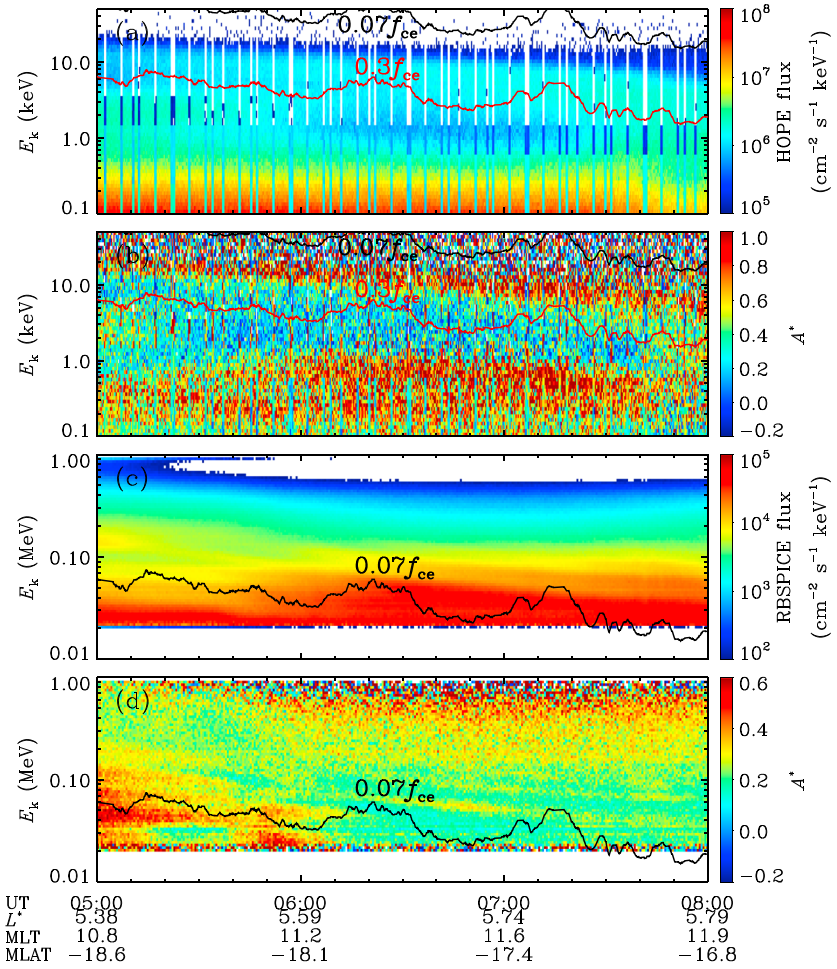

Figure 4. (a) Helium, oxygen, proton, and electron omnidirectional electron flux; (b) the corresponding electron anisotropy; (c) Radiation Belt Storm Probes Ion Composition Experiment omnidirectional electron flux; and (d) the electron anisotropy as a function of time and energy. The black solid and red solid lines represent the minimum energies of electron resonating with waves of frequencies 0.07 f_{ce} and 0.3 f_{ce} via fundamental cyclotron resonance.

$$\eta = \pi\mu_h \frac{(\omega_r - |\Omega_e|)}{k} \int_0^\infty \frac{p_\perp^2 dp_\perp}{\Delta_R} \frac{\partial F}{\partial p_\perp}\Big|_{p_\parallel = p_R} \tag{2}$$

is the fraction of the electron distribution near resonance,

$$A = \frac{\frac{k}{(\omega_r - |\Omega_e|)} \int_0^\infty \frac{dp_\perp}{\Delta_R} \frac{p_\perp^2}{\gamma_R} \left(p_\perp \frac{\partial F}{\partial p_\parallel} - p_\parallel \frac{\partial F}{\partial p_\perp} \right)}{\int_0^\infty \frac{dp_\perp}{\Delta_R} p_\perp^2 \frac{\partial F}{\partial p_\perp}} \Big|_{p_\parallel = p_R} \tag{3}$$

is the dimensionless measure of the relativistic pitch angle anisotropy of the resonant particles, and

$$A_c = \omega_r / \left(|\Omega_e| - \omega_r \right) \tag{4}$$

is the threshold anisotropy for whistler mode excitation. Here ω_r is the real part of complex wave frequency; ω_{pe} is the electron plasma frequency; Ω_e is the angular gyrofrequency of electron; $p_R = (\gamma_R \omega_r - |\Omega_e|)/k$ is the resonant electron parallel momentum for the fundamental cyclotron resonance; γ_R is the relativistic factor of the resonant electrons; k is the wave number; $p_\parallel$ and $p_\perp$ are the parallel and perpendicular components of electron momentum, respectively; F is the normalized electron distribution function; $\Delta_R = 1 - \omega_r P_R/(c^2 k \gamma_R)$ is a strictly positive quantity; c is the speed of light; and μ_h is the density ratio between the hot and cold electrons.

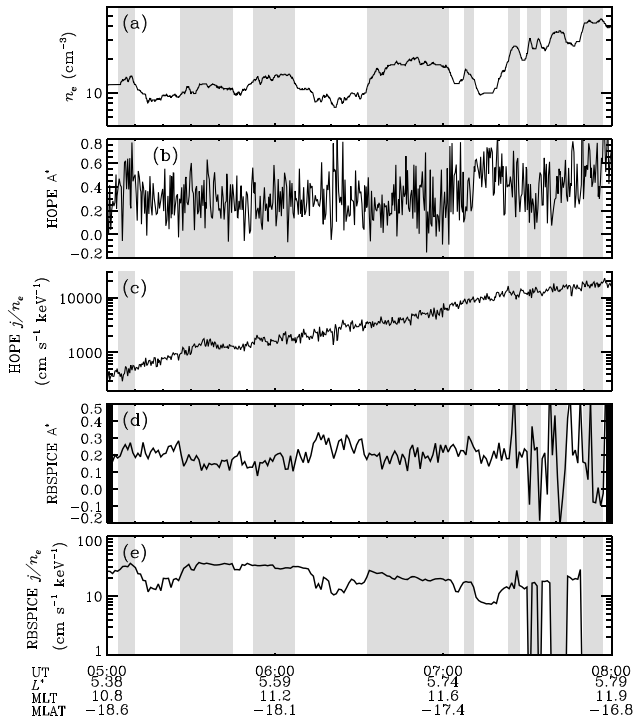

Figure 5. (a) Electron number density derived from high-frequency receiver channel; (b) the electron anisotropy and (c) the ratio of omnidirectional electron flux to the electron number density at the minimum energies of electron resonating with wave of frequency 0.3 f_{ce} based on the helium, oxygen, proton, and electron (HOPE); and (d) the electron anisotropy and (e) the ratio of omnidirectional electron flux to the electron number density at the minimum energies of electron resonating with wave of frequency 0.07 f_{ce} based on the Radiation Belt Storm Probes Ion Composition Experiment (RBSPICE). MLT = magnetic local time.

According to equation (1) the growth rate ω_i is proportional to η, and its sign depends on A. When $A > A_c$, the value of ω_i is positive (wave growth). When $A < A_c$, the value of ω_i is negative (wave damping). It should be noted that both integrals for both the fraction η and the anisotropy A require the full distribution function. Obviously, it is not convenient to obtain η and A values from the in situ measurements due to the different instruments measuring the limited energy ranges and their intercalibrations. Hence, in the following analysis we provide two similar quantities to estimate the fraction and pitch angle anisotropy instead of η and A. The fraction of resonant electron to total electron is characterized by j/n_e (Zhu et al., 2015), where j is the measured omnidirectional flux at the minimum energy and n_e is the cold electron number density. Electron pitch angle anisotropy (A^*) at a fixed kinetic energy (Chen et al., 1998; Li, Bortnik, Thorne, & Angelopoulos, 2011) is defined as follows:

$$A^* = \frac{\int_0^\pi F(E_k,\alpha)\sin^3\alpha d\alpha}{2\int_0^\pi F(E_k,\alpha)\cos^2\alpha\sin\alpha d\alpha} - 1, \quad (5)$$

where E_k is the electron kinetic energy and α is the local pitch angle. $A^* = 0$ represents isotropic pitch angle distribution. $A^* > 0$ means anisotropic pitch angle distribution with peak at $\alpha = 90°$, while $A^* < 0$ means anisotropic pitch angle distribution with minimum at $\alpha = 90°$.

Figures 4a and 4b show the omnidirectional electron fluxes measured by the helium, oxygen, proton, and electron (HOPE) mass spectrometer (Funsten et al., 2013) onboard the Van Allen Probes and the corresponding electron pitch angle anisotropies A^* obtained from unidirectional fluxes observation. Figures 4c and 4d present the omnidirectional fluxes measured by the Radiation Belt Storm Probes Ion Composition Experiment (RBSPICE; Mitchell et al., 2013) and the pitch angle anisotropies A^*. Here we do not use the magnetic electron ion spectrometer (Blake et al., 2013) data, which also are part of energetic particle composition & thermal plasma suite (Spence et al., 2013). That is because that RBSPICE provides higher-resolution energetic electron observation with 17 points in pitch angle range from 7.5° to 172.5° and 64 points in energy range from 20 to 939 keV. Hereinafter we will analyze HOPE data and RBSPICE data separately in order to avoid intercalibration between the two instruments. The two solid lines represent the minimum resonance energies for the two frequencies $0.07f_{ce}$ and $0.3f_{ce}$, by simultaneously solving dispersion relation (Stix, 1992) and cyclotron resonance condition using the real-time magnetic intensity data and number density identified by NURD. We can see that HOPE observations cover the energy range from 0.1 to 10 keV. In the energy range [0.1, 1] keV the electrons present high anisotropic with $A^* \sim 0.8$. In the energy range [1, 10] keV the electrons show weak anisotropy with $0 < A^* \leq 0.3$for most of time. Figures 4c and 4d present the RBSPICE observations covering the range from 20 keV to 1 MeV. The corresponding anisotropy values are roughly larger than 0.2. HOPE data capture the variability of electrons resonant with chorus wave at $0.3f_{ce}$, and RBSPICE data capture the variability of electron resonant with exohiss wave at $0.07f_{ce}$. Both the minimum resonance energies for $0.07f_{ce}$ and $0.3f_{ce}$ fluctuated with the fluctuation of electron number density. Particularly, the minimum resonance energies exhibited the out-phase variation with electron density. That is because the variation of electron density essentially influences the dispersion relation and therefore the cyclotron resonance. In addition, it is interesting to note that chorus waves cyclotron-resonate with 1- to 10-keV electrons while exohiss waves cyclotron-resonate with 10- to 100-keV electrons in this case.

Figure 5a is the same as Figure 3a, showing discrete enhancements of electron number density. The gray regions are selected to highlight the enhancement of electron number density. Figures 5b and 5c show the electron pitch angle anisotropy and the ratio of omnidirectional electron flux to the electron number density at the minimum energies of electron resonating with wave of frequency 0.3 f_{ce} based on the HOPE

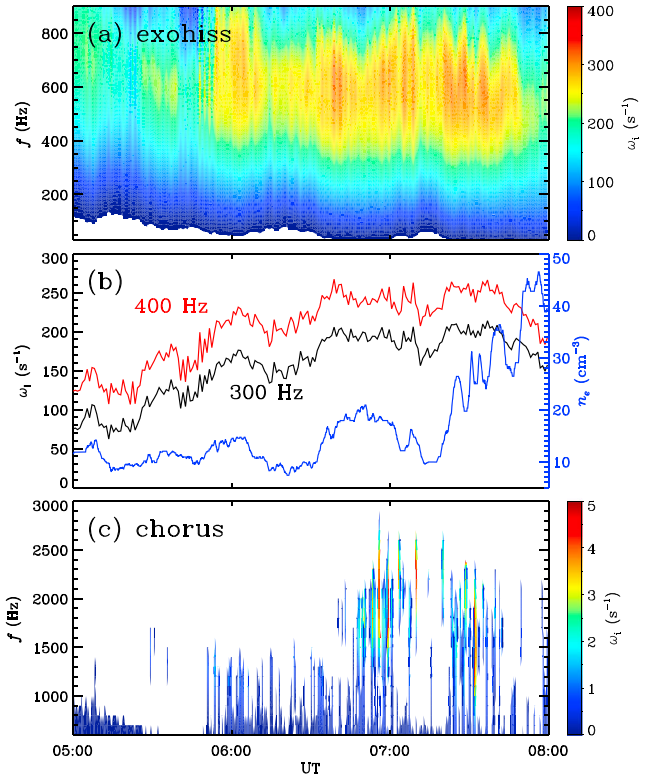

Figure 6. (a) growth rates of parallel exohiss waves as functions of time and frequency based on Radiation Belt Storm Probes Ion Composition Experiment observation; (b) growth rate profiles of 300 Hz (black solid line) and 400 Hz (red solid line) exohiss waves and electron density number of profile (blue solid line); (c) growth rates of parallel chorus waves based on helium, oxygen, proton, and electron electron distribution.

observations. Obviously, most of the anisotropies A^* are larger than 0.2, indicating the possibility of exciting whistler mode wave. Although the values of electron anisotropy exhibit high-frequency fluctuations, they do not show a good correlation with the variability of number density. The ratios of omnidirectional flux to number density j/n_e tend to increase by 2 orders of magnitude but show some in-phase fluctuation with the variation of number density. Figures 5d and 5e plot the electron anisotropy and the ratio of the omnidirectional electron flux to the electron density at the minimum energies of electron resonating with wave of frequency 0.07 f_{ce} based on the RBSPICE measurements. The values of anisotropy A^* for 0.07 f_{ce} are larger than 0.1 except the time after UT 07:30. Looking at Figure 4d, the minimum energies of electron can lower down to 15 keV, which is smaller than the minimum of observed energy range by RBSPICE. Hence, the A^* and j/n_e are not accurate after UT 07:30. We can see that the values of A^* vary but do not show good correlation with number density variations. Compared with this good correlation between density and the ratio j/n_e observed by RBSPICE, the corresponding correlation observed by HOPE is relatively poor, which possibly caused by the low-resolution energy sampling. During the following growth rate calculation, we will use HOPE and RBSPICE data to verify the correlation between density variation and exohiss and chorus amplification, respectively. In addition, the ratios j/n_e show a well-positive correlation with number density, which means the plasma is capable of providing more free energy with the enhancement of number density. Note that the increase of n_e leads to the decrease of resonance energy and thus the increase of j at resonant energy. This explains j/n_e increases with n_e shown.

3. Calculation of Growth Rates

After the above analysis on plasma data, we calculate the linear growth rates (Xiao et al., 1998) of parallel whistler waves based on RBSPICE and HOPE electron distributions. Figures 6a and 6b show growth rates of parallel exohiss waves based on RBSPICE electron distribution, and Figure 6c shows growth rate of parallel chorus waves based on HOPE electron distribution. We can see that both the growth rates of exohiss and chorus waves tend to increase during density enhancement and decrease during density depletion. As shown, the values of growth rates vary in positive correlation with density variations, which is consistent with our analysis on plasma data. It should be noted that the peak of exohiss growth rates at fixed time is always located around 600–700 Hz rather than the typical frequency of exohiss waves ~300 Hz. The frequency distribution of exohiss growth rates directly results from the observed plasma distribution function and its lower and upper energy cutoffs. The inconsistency between observed low-frequency, narrow-banded exohiss waves and simulated high-frequency, wide-banded growth rate distribution can be explained by the following two reasons. First, the seed population of exohiss emission, plasmaspheric hiss, is low frequency and narrow banded. A recent study (Li et al., 2015) found that at different L regions and under different geomagnetic conditions, the frequency of the plasmaspheric hiss averaged wave power peak closes to 300 Hz. When hiss leaks, the exohiss waves show the similar frequency distribution. Second, the process of leaking through the plasmasphere may be also frequency dependent. It should be noted that for both the particle analysis and wave growth rate calculation, all parameters we adopted (e.g., electron number density, electron distributions, and background magnetic fields) are local parameters and therefore the corresponding anisotropy and growth rates are local too. One may obtain the equatorial parameters by mapping the observed distribution into that at the magnetic equator with near 90° degree equatorial pitch angle missing. In our event both the local anisotropy and calculated growth rate suggest that the local plasma environment event at latitude −17° is capable of providing free energy for wave excitation and therefore the equatorial region can be more unstable.

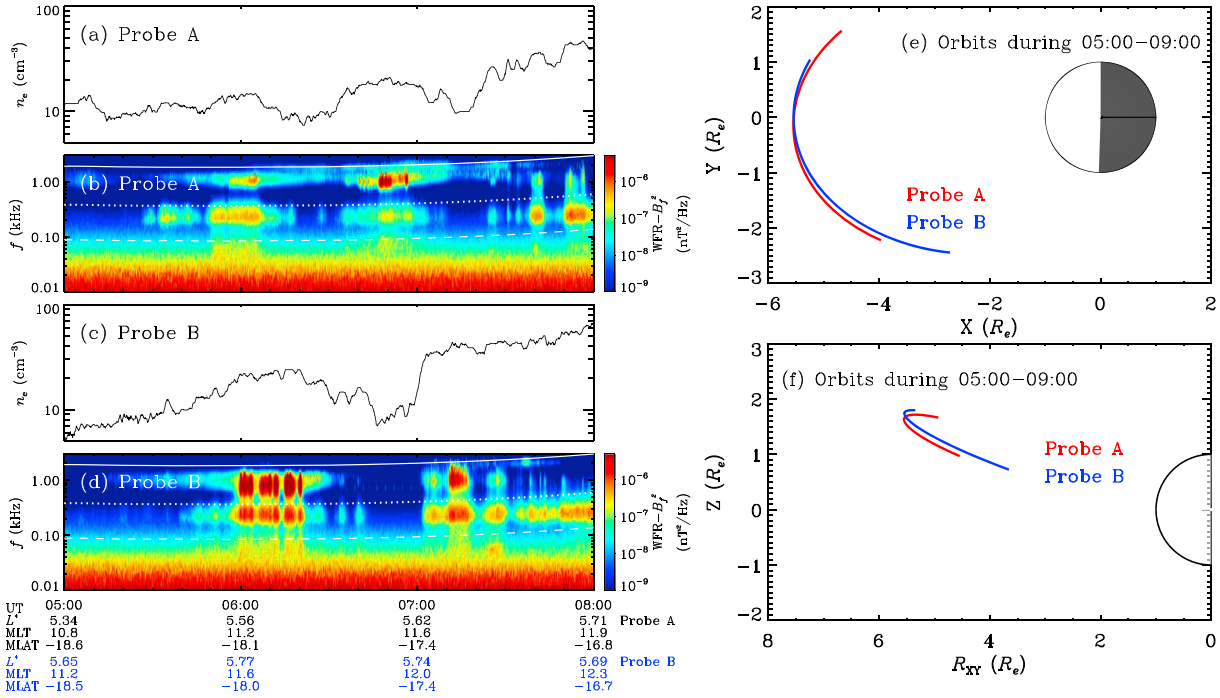

Figure 7. Van Allen Probe A: (a) electron number density and (b) magnetic power spectral densities; Van Allen Probe B: (c) electron number density, (d) magnetic power spectral densities, and (e, f) the orbits of Probe A (red solid lines) and Probe B (blue solid lines) during UT 05:00–09:00 on 26 February 2014 projected in the *X*-*Y* plane and in the R_{xy}-*Z* plane of solar magnetosphere coordinate system. MLT = magnetic local time; WFR = waveform receiver.

4. Discussions

In the above context, we describe the in situ observation measured by Van Allen Probe A containing the variations of electron number density, exohiss, and chorus wave amplitudes and their positive correlation. We then use the plasma measurements to explain that the amplification of waves; particularly, exohiss wave is due to the decrease of resonant energy caused by the number density enhancement and thus takes place when plasma density enhances. The calculated growth rate of exohiss wave shows the positive correlation with electron density supporting our explanation. The observed correlations among in situ parameters tend to exclude this possibility that the exohiss waves have been amplified inside the plasmasphere during the density enhancement before leaking outside as suggested by Li et al. (2013). For this case to occur the good correlation between density variation outside plasmapause and exohiss amplitude requires that the density variation structure has to cover a huge spatial range to make sure the in-phase correlation between the density variation outside and inside the plasmasphere. Here we use twin Van Allen Probes to investigate the spatial range of density variation. Figure 7 shows the electron density, magnetic power spectral densities for exohiss, and chorus measured by twin Van Allen Probes and their orbits projected in the *X*-*Y* plane and in the R_{xy}-*Z* plane of solar magnetosphere coordinate system. We can see Probe B had similar trajectory with Probe A, flying from prenoon sector to duskside sector at $L \sim 5.7$ and outside the plasmasphere. The positive correlation between density enhancement and wave power has also been clearly observed. However, the density profiles observed by the two probes are significantly different from each other. At UT 06:10, the density observed by Probe B reached peak while the density from Probe A was significantly decreasing. At UT 06:50, the density observed by Probe B was much small, located between two peaks, while the density observed by Probe A was at peak. At UT 07:20, the density observed by Probe A started to increase, but the density observed by Probe B did not change much. So the spatial scale of density structure is smaller than 0.09 R_e, and thus, we can exclude the possible scenario that exohiss have been intensified inside plasmasphere before leakage.

Besides the amplification of exohiss due to electron enhancement, the chorus waves also exhibit similar amplification. The growth rate calculation confirms the effects of density variation. Moreover, the obliqueness of chorus changed with electron density variation. As shown in Figures 2b and 2e, intense chorus waves (~1 kHz) have parallel propagation direction, while some with much weaker intensity can be oblique. During the density enhancement, chorus waves became more intensive and more parallel, which indicates the increased

growth rate of parallel propagation. The generation of oblique chorus has been also investigated by previous studies (Artemyev et al., 2016; Li et al., 2016; Mourenas et al., 2015).

5. Conclusions

In this work, we report an event when exohiss and chorus waves outside the plasmapause were simultaneous intensified observed by the Van Allen Probe A, which occurred during the late recovery phase of a weak geomagnetic storm. Exohiss waves below $0.1f_{ce}$ were identified with equatorward Poynting fluxes, while chorus waves within $[0.1f_{ce}, 0.5f_{ce}]$ frequency range were identified with poleward Poynting fluxes. The characteristics of Poynting fluxes suggest that exohiss results from the leakage of plasmaspheric hiss while chorus originates from the minimum region of magnetic field outside the plamasphere via cyclotron resonance instability. The minimum resonant energies for exohiss and chorus waves calculated by solving dispersion relation and fundamental cyclotron resonance show that chorus waves are mainly associated with 1- to 10-keV suprethermal electrons while exohiss is associated with 20- to 400-keV energetic electrons. Both their amplitudes presented in-phase correlation with electron number density, which is obtained by NURD algorithm. To investigate possible mechanism, the linear theory of relativistic plasma is adopted to analyze plasma pitch angle anisotropy and the fraction of resonant electron to total electron from plasma observed by HOPE and RBSPICE instruments. Sufficient pitch angle anisotropies at the minimum energies of electron resonating with both chorus and exohiss waves allow their excitation. The in-phase enhancements of the resonant electron fraction with number density particularly for exohiss waves indicate that more free energies for wave generation are available during the high-density periods, which can well explain the intensification of exohiss. Furthermore, the calculation of corresponding growth rates further supports that with pitch angle anisotropic resonant electrons, the density enhancements cause the increase of growth rates and then exohiss intensity amplification. These results suggest that exohiss waves have potential to play a more important role due to the background plasma fluctuation.

The present study focuses on the local growth of exohiss caused by background fluctuation, while wave propagation is also important. Ray tracing method, which simulates the wave propagation path and the wave gain accumulated along the path, requires the global cold electron density model, suprethermal electron distribution, and the wave source (Chen et al., 2012a, 2012b; Horne, 1989). Ray tracing simulation with density ducts has been shown previously (Chen, Thorne, et al., 2012). For example, Figure 4 of Chen, Thorne, et al. (2012) demonstrates that with the presence of density enhancement ducts, whistler mode can be trapped and exhibit parallel propagation. Because raypath is reversible, one can expect that escaped hiss emission (exohiss) can be guided along the density duct toward the equator. In addition to this ducting effect, one may also expect the preferred amplification for parallel propagation. Both reasons favor parallel propagation as observed. Additionally, the ray tracing simulation (Bortnik et al., 2008; Chen et al., 2012a, 2012b) suggests that chorus waves generated near the magnetic equator, if not entering the plasmasphere to avoid strong damping, hardly experience magnetospheric reflection because of strong Landau damping outside the plasmapause and thus unlikely return wave energy toward the equator. These results also support that exohiss waves originate from escape of plasmaspheric hiss waves (Zhu et al., 2015).

Acknowledgments
The authors used geomagnetic indices provided by OMNIWeb (http://omniweb.gsfc.nasa.gov/form/dx1.html). This research was supported by the NSF Grants AGS-1203747 and AGS-1405041 and NASA Grants NNX13AE34G, NNX10AK99, and NNX15AF55G. This project also received support from the Progress H2020 Grant 637302.

References

Artemyev, A., Agapitov, O., Mourenas, D., Krasnoselskikh, V., Shastun, V., & Mozer, F. (2016). Oblique Whistler-mode waves in the Earth's inner magnetosphere: Energy distribution, origins, and role in radiation belt dynamics. *Space Science Reviews*, *200*, 261–355. https://doi.org/10.1007/s11214-016-0252-5

Blake, J. B., Carranza, P. A., Claudepierre, S. G., Clemmons, J. H., Crain, W. R. Jr, Dotan, Y., et al. (2013). The magnetic electron ion spectrometer (MagEIS) instruments aboard the Radiation Belt Storm Probes (RBSP) spacecraft. *Space Science Reviews*, *179*, 383–421. https://doi.org/10.1007/s11214-013-9991-8

Bortnik, J., Thorne, R. M., & Meredith, N. P. (2008). The unexpected origin of plasmaspheric hiss from discrete chorus emissions. *Nature*, *452*, 62–66. https://doi.org/10.1038/nature06741

Burtis, W. J., & Helliwell, R. A. (1969). Banded chorus—A new type of VLF radiation observed in the magnetosphere by OGO 1 and OGO 3. *Journal of Geophysical Research*, *74*(11), 3002–3010. https://doi.org/10.1029/JA074i011p03002

Chen, L., Bortnik, J., Li, W., Thorne, R. M., & Horne, R. B. (2012a). Modeling the properties of plasmaspheric hiss: 1. Dependence on chorus wave emission. *Journal of Geophysical Research*, *117*, A05201. https://doi.org/10.1029/2011JA017201

Chen, L., Bortnik, J., Li, W., Thorne, R. M., & Horne, R. B. (2012b). Modeling the properties of plasmaspheric hiss: 2. Dependence on the plasma density distribution. *Journal of Geophysical Research*, *117*, A05202. https://doi.org/10.1029/2011JA017202

Chen, M. W., Roeder, J. L., Fennell, J. F., Lyons, L. R., & Schulz, M. (1998). Simulations of ring current proton pitch angle distributions. *Journal of Geophysical Research*, *103*, 165–178. https://doi.org/10.1029/97JA02633

Chen, L., Thorne, R. M., Li, W., Bortnik, J., Turner, D., & Angelopoulos, V. (2012). Modulation of plasmaspheric hiss intensity by thermal plasma density structure,. *Geophysical Research Letters*, *39*, L14103. https://doi.org/10.1029/2012GL052308

Funsten, H. O., Skoug, R. M., Guthrie, A. A., MacDonald, E. A., Baldonado, J. R., Harper, R. W., et al. (2013). Helium, oxygen, proton, and electron (HOPE) mass spectrometer for the Radiation Belt Storm Probes Mission. *Space Science Reviews*, *179*, 423–484. https://doi.org/10.1007/s11214-013-9968-7

Helliwell, R. A. (1967). A theory of discrete VLF emissions from the magnetosphere. *Journal of Geophysical Research*, *72*(19), 4773–4790. https://doi.org/10.1029/JZ072i019p04773

Horne, R. B. (1989). Path-integrated growth of electrostatic waves: The generation of terrestrial myriametric radiation. *Geophysical Research Letters*, *94*, 8895–8909. https://doi.org/10.1029/JA094iA07p08895

Horne, R. B., & Thorne, R. M. (1998). Potential waves for relativistic electron scattering and stochastic acceleration during magnetic storms. *Geophysical Research Letters*, *25*, 3011–3014. https://doi.org/10.1029/98GL01002

Kennel, C. F., & Petschek, H. E. (1966). Limit on stably trapped particle fluxes. *Journal of Geophysical Research*, *71*, 1–28.

Kletzing, C. A., Kurth, W. S., Acuna, M., MacDowall, R. J., Torbert, R. B., Averkamp, T., et al. (2013). The electric and magnetic field instrument suite and integrated science (EMFISIS) on RBSP. *Space Science Reviews*, *179*, 127–181. https://doi.org/10.1007/s11214-013-9993-6

Li, W., Bortnik, J., Thorne, R. M., & Angelopoulos, V. (2011). Global distribution of wave amplitudes and wave normal angles of chorus waves using THEMIS wave observations. *Journal of Geophysical Research*, *116*, A12205. https://doi.org/10.1029/2011JA017035

Li, W., Bortnik, J., Thorne, R. M., Nishimura, Y., Angelopoulos, V., & Chen, L. (2011). Modulation of whistler mode chorus waves: 2. Role of density variations. *Journal of Geophysical Research*, *116*, A06206. https://doi.org/10.1029/2010JA016313

Li, W., Ma, Q., Thorne, R. M., Bortnik, J., Kletzing, C. A., Kurth, W. S., et al. (2015). Statistical properties of plasmaspheric hiss derived from Van Allen Probes data and their effects on radiation belt electron dynamics. *Journal of Geophysical Research: Space Physics*, *120*, 3393–3405. https://doi.org/10.1002/2015JA021048

Li, W., Mourenas, D., Artemyev, A. V., Bortnik, J., Thorne, R. M., Kletzing, C. A., et al. (2016). Unraveling the excitation mechanisms of highly oblique lower band chorus waves. *Geophysical Research Letters*, *43*, 8867–8875. https://doi.org/10.1002/2016GL070386

Li, W., Thorne, R. M., Bortnik, J., Reeves, G. D., Kletzing, C. A., Kurth, W. S., et al. (2013). An unusual enhancement of low-frequency plasmaspheric hiss in the outer plasmasphere associated with substorm-injected electrons. *Geophysical Research Letters*, *40*, 3798–3803. https://doi.org/10.1002/grl.50787

Mauk, B. H., Fox, N. J., Kanekal, S. G., Kessel, R. L., Sibeck, D. G., & Ukhorskiy, A. (2013). Science objectives and rationale for the Radiation Belt Storm Probes Mission. *Space Science Reviews*, *179*, 3–27. https://doi.org/10.1007/s11214-012-9908-y

Meredith, N. P., Horne, R. B., & Anderson, R. R. (2001). Substorm dependence of chorus amplitudes: Implications for the acceleration of electrons to relativistic energies. *Journal of Geophysical Research*, *106*, 13,165–13,178. https://doi.org/10.1029/2000JA900156

Mitchell, D. G., Lanzerotti, L. J., Kim, C. K., Stokes, M., Ho, G., Cooper, S., et al. (2013). Radiation Belt Storm Probes Ion Composition Experiment (RBSPICE). *Space Science Reviews*, *179*, 263–308. https://doi.org/10.1007/s11214-013-9965-x

Moullard, O., Masson, A., Laakso, H., Parrot, M., Dcrau, P., Santolik, O., & Andre, M. (2002). Density modulated whistler mode emissions observed near the plasmapause. *Geophysical Research Letters*, *29*(20), 1975. https://doi.org/10.1029/2002GL015101

Mourenas, D., Artemyev, A. V., Agapitov, O. V., Krasnoselskikh, V., & Mozer, F. S. (2015). Very oblique whistler generation by low-energy electron streams. *Journal of Geophysical Research: Space Physics*, *120*, 3665–3683. https://doi.org/10.1002/2015JA021135

Ni, B., Thorne, R. M., Shprits, Y. Y., & Bortnik, J. (2008). Resonant scattering of plasma sheet electrons by whistler-mode chorus: Contribution to diffuse auroral precipitation. *Geophysical Research Letters*, *35*, L11106. https://doi.org/10.1029/2008GL034032

Nishimura, Y., Bortnik, J., Li, W., Thorne, R. M., Lyons, L. R., Angelopoulos, V., et al. (2010). Identifying the driver of pulsating aurora. *Science*, *330*(6000), 81–84. https://doi.org/10.1126/science.1193186

Nunn, D., Omura, Y., Matsumoto, H., Nagano, I., & Yagitani, S. (1997). The numerical simulation of VLF chorus and discrete emissions observed on the Geotail satellite using a Vlasov code. *Journal of Geophysical Research*, *102*, 27,083–27,098. https://doi.org/10.1029/97JA02518

Reeves, G. D., Spence, H. E., Henderson, M. G., Morley, S. K., Friedel, R. H., Funsten, H. O., et al. (2013). Electron acceleration in the heart of the Van Allen radiation belts. *Science*, *341*(6149), 991–994. https://doi.org/10.1126/science.1237743

Shprits, Y. Y., Subbotin, D. A., Meredith, N. P., & Elkington, S. R. (2008). Review of modeling of losses and sources of relativistic electrons in the outer radiation belt II: Local acceleration and loss. *Journal of Atmospheric and Solar-Terrestrial Physics*, *70*, 1694–1713. https://doi.org/10.1016/j.jastp.2008.06.014

Spence, H. E., Reeves, G. D., Baker, D. N., Blake, J. B., Bolton, M., Bourdarie, S., et al. (2013). Science goals and overview of the Radiation Belt Storm Probes (RBSP) energetic particle, composition, and thermal plasma (ECT) suite on NASA's Van Allen Probes Mission. *Space Science Reviews*, *179*, 311–336. https://doi.org/10.1007/s11214-013-0007-5

Stix, T. H. (1992). *Waves in plasmas*. New York: American Institute of Physics.

Summers, D., Ma, C., Meredith, N. P., Horne, R. B., Thorne, R. M., Heynderickx, D., & Anderson, R. R. (2002). Model of the energization of outer-zone electrons by whistler-mode chorus during the October 9, 1990 geomagnetic storm. *Geophysical Research Letters*, *29*(24), 2174. https://doi.org/10.1029/2002GL016039

Summers, D., Ni, B., & Meredith, N. P. (2007). Timescales for radiation belt electron acceleration and loss due to resonant wave-particle interactions: 2. Evaluation for VLF chorus, ELF hiss, and electromagnetic ion cyclotron waves. *Journal of Geophysical Research*, *112*, A04207. https://doi.org/10.1029/2006JA011993

Thorne, R. M. (2010). Radiation belt dynamics: The importance of wave-particle interactions. *Geophysical Research Letters*, *37*, L22107. https://doi.org/10.1029/2010GL044990

Thorne, R. M., Smith, E. J., Burton, R. K., & Holzer, R. E. (1973). Plasmaspheric hiss. *Journal of Geophysical Research*, *78*, 1581–1596. https://doi.org/10.1029/JA078i010p01581

Tsurutani, B. T., & Smith, E. J. (1974). Postmidnight chorus: A substorm phenomenon. *Journal of Geophysical Research*, *79*, 118–127. https://doi.org/10.1029/JA079i001p00118

Tsurutani, B. T., & Smith, E. J. (1977). Two types of magnetospheric ELF chorus and their substorm dependences. *Journal of Geophysical Research*, *82*, 5112–5128. https://doi.org/10.1029/JA082i032p05112

Turner, D. L., Angelopoulos, V., Li, W., Bortnik, J., Ni, B., Ma, Q., et al. (2014). Competing source and loss mechanisms due to wave-particle interactions in Earth's outer radiation belt during the 30 September to 3 October 2012 geomagnetic storm. *Journal of Geophysical Research: Space Physics*, *119*, 1960–1979. https://doi.org/10.1002/2014JA019770

Turner, D. L., Angelopoulos, V., Morley, S. K., Henderson, M. G., Reeves, G. D., Li, W., et al. (2014). On the cause and extent of outer radiation belt losses during the 30 September 2012 dropout event. *Journal of Geophysical Research: Space Physics*, *119*, 1530–1540. https://doi.org/10.1002/2013JA019446

Xiao, F., Thorne, R. M., & Summers, D. (1998). Instability of electromagnetic R-mode waves in a relativistic plasma. *Physics of Plasmas*, *5*, 2489.

Xiao, F., Yang, C., He, H., Su, Z., Zhou, Q., He, Y., et al. (2014). Chorus acceleration of radiation belt relativistic electrons during March 2013 geomagnetic storm. *Journal of Geophysical Research: Space Physics*, *119*, 3325–3332. https://doi.org/10.1002/2014JA019822

Zhelavskaya, I. S., Spasojevic, M., Shprits, Y. Y., & Kurth, W. S. (2016). Automated determination of electron density from electric field measurements on the van allen probes spacecraft. *Journal of Geophysical Research: Space Physics*, *121*, 4611–4625. https://doi.org/10.1002/2015JA022132

Zhu, H., Su, Z., Xiao, F., Zheng, H., Wang, Y., Shen, C., et al. (2015). Plasmatrough exohiss waves observed by Van Allen Probes: Evidence for leakage from plasmasphere and resonant scattering of radiation belt electrons. *Geophysical Research Letters*, *42*, 1012–1019. https://doi.org/10.1002/2014GL062964